Partially Folded Intermediates as Critical Precursors of Light Chain Amyloid Fibrils and Amorphous Aggregates†

Ritu Khurana, Joel R. Gillespie,‡ Anupam Talapatra, Lauren J. Minert, Cristian Ionescu-Zanetti, Ian Millett,‡ and Anthony L. Fink*

Department of Chemistry and Biochemistry, University of California, Santa Cruz, California 95064

Received July 31, 2000; Revised Manuscript Received January 22, 2001

ABSTRACT: Light chain, or AL, amyloidosis is a pathological condition arising from systemic extracellular deposition of monoclonal immunoglobulin light chain variable domains in the form of insoluble amyloid fibrils, especially in the kidneys. Substantial evidence suggests that amyloid fibril formation from native proteins occurs via a conformational change leading to a partially folded intermediate conformation, whose subsequent association is a key step in fibrillation. In the present investigation, we have examined the properties of a recombinant amyloidogenic light chain variable domain, SMA, to determine whether partially folded intermediates can be detected and correlated with aggregation. The results from spectroscopic and hydrodynamic measurements, including far- and near-UV circular dichroism, FTIR, NMR, and intrinsic tryptophan fluorescence and small-angle X-ray scattering, reveal the build-up of two partially folded intermediate conformational states as the pH is decreased (low pH destabilized the protein and accelerated the kinetics of aggregation). A relatively nativelike intermediate, I_N, was observed between pH 4 and 6, with little loss of secondary structure, but with significant tertiary structure changes and enhanced ANS binding, indicating exposed hydrophobic surfaces. At pH below 3, we observed a relatively unfolded, but compact, intermediate, I_U, which was characterized by decreased tertiary and secondary structure. The I_U intermediate readily forms amyloid fibrils, whereas I_N preferentially leads to amorphous aggregates. Except at pH 2, where negligible amorphous aggregate is formed, the amorphous aggregates formed significantly more rapidly than the fibrils. This is the first indication that different partially folded intermediates may be responsible for different aggregation pathways (amorphous and fibrillar). The data support the hypothesis that amyloid fibril formation involves the ordered self-assembly of partially folded species that are critical soluble precursors of fibrils.

Immunoglobulin (Ig)[1] light chains are involved in several protein deposition diseases, including one resulting in the formation and deposition of amyloid fibrils (light chain or AL amyloidosis) and another known as light chain deposition disease that involves amorphous protein deposits (*1*, *2*). The morphology of the deposited aggregates in these two diseases is clearly different, and typically patients exhibit only one form of light chain deposition. However, there is at least one report of a patient exhibiting both AL amyloidosis and LCDD involving the same light chain (*3*). The exact length of light chains in amyloid deposits varies, but is usually in the 110−130 residue range (12−14 kDa) corresponding to the intact variable domain (*4*).

The molecular mechanisms leading to amyloid formation are poorly understood. In this report, we address the question of why some immunoglobulin light chains form amyloid and related deposits while others do not, in particular the hypothesis that protein aggregation arises from the self-association of partially folded intermediates. Support for this hypothesis has been found with proteins such as transthyretin (*5*) and lysozyme (*6*). We postulate that amyloid fibril formation from native proteins occurs via a conformational change leading to formation of a partially folded intermediate conformation, association of this intermediate to form soluble oligomers leading to the critical nucleus, and subsequent formation of the initial fibrillar species, typically a filament or protofibril, and finally association of protofibrils into mature fibrils (*7*).

We have investigated the biophysical properties and amyloidogenicity of the variable domain of a recombinant amyloidogenic light chain, SMA, engineered by Stevens et al. (*8*). SMA (114 residues, M_r = 12 700) was initially

† This research was supported by grants from the National Institutes of Health and the University of California Systemwide Biotechnology Research and Education Program. Small-angle X-ray scattering data were collected at Beam Line 4-2, Stanford Synchrotron Radiation Laboratory (SSRL). SSRL is supported by the U.S. Department of Energy, Office of Basic Energy Sciences, and in part by the National Institutes of Health, National Center for Research Resources, Biomedical Technology Program, and by the Department of Energy, Office of Biological and Environmental Research.

* Correspondence should be addressed to this author at the Department of Chemistry and Biochemistry, University of California, Santa Cruz, CA 95064. Tel: (831) 459-2744; Fax: (831) 459-2935; E-mail: enzyme@cats.ucsc.edu.

‡ Current address: Department of Chemistry, Stanford University, Stanford, CA 94305.

[1] Abbreviations: SAXS, small-angle X-ray scattering; R_g, radius of gyration; FTIR, Fourier transform infrared spectroscopy; ATR, attenuated total reflectance; IRE, internal reflectance element; TEM, transmission electron microscopy; AFM, atomic force microscopy; TFT, Thioflavin T; ANS, 8-anilino-1-naphthalenesulfonate; CD, circular dichroism; Ig, immunoglobulin; V_L, variable domain of Ig light chain.

10.1021/bi001782b CCC: $20.00
Published on Web 03/02/2001

extracted from lymph node-derived amyloid fibrils of an AL amyloidosis patient (*9*). A very similar light chain domain, LEN, was derived from a patient with multiple myeloma who showed no evidence of renal dysfunction or amyloidosis (*10*). The IgG-V_L domains consist of a highly conserved framework formed by two sheets of antiparallel β-strands forming a β-sandwich, and three loops comprising the complementarity-determining regions (CDR) that form part of the antigen binding site. The sequences of SMA and LEN are very similar, differing only at 8 positions out of 114. Four of these are in CDR3 (Q89H, T94H, Y96Q, S97T), two are in CDR1 (S29N, K30R), and the remaining two are in the framework region (P40L, I106L). The high-resolution crystallographic structure of LEN (1.8 Å) has been solved (PDB Accession No. 1LVE) (*11*). Both SMA and LEN belong to the κIV family of Igs.

The amyloidogenic light chain, SMA, is significantly less thermodynamically stable than LEN under all conditions (unpublished observations). The presence of low concentrations of denaturants also results in fibril formation from the "benign" LEN (*12*). In the present study, we used biophysical characterization of the conformation of SMA as a function of pH to reveal the presence of two distinct partially folded intermediates: one with relatively nativelike properties, the other with relatively unfolded properties. Destabilizing conditions at physiological pH, e.g., low urea concentration, also lead to aggregation and fibril formation. Thus, conditions that result in population of these intermediates lead to aggregation, supporting the hypothesis that partially folded intermediates are key precursors on the aggregation pathway. Interestingly, both amorphous and fibrillar aggregates were observed, and were shown to arise from two different intermediates.

MATERIALS AND METHODS

Expression and Purification of Recombinant V_L SMA. The recombinant V_L domain SMA was purified from JM83 *E. coli* cells transformed with the plasmid pkIVsma004, generously provided by Dr. Fred Stevens, Argonne National Lab (*8*). The plasmid construct was based on the pASK vectors constructed by Skerra et al. (*13*) and contained an *ompA* leader for periplasmic localization of the protein to ensure the formation of the core disulfide bond. The overexpressed protein was purified using the procedure of Stevens et al. (*8*) with minor modifications. Briefly, the recombinant protein was extracted from the periplasm using osmotic shock via treatment with ice-cold TES followed by distilled water. The periplasmic extract was dialyzed against 4 changes of 20 volumes of 10 mM acetate buffer, pH 5.6, and loaded onto a fast-flow SP Sepharose column. The column was washed with 10 mM acetate buffer, pH 5.6, and the protein eluted using 10 mM phosphate buffer, pH 8.0. The fractions were assayed by SDS−PAGE, and fractions containing the recombinant protein were pooled, filtered through 0.22 μm filters, and stored in glass vials. Typical yields were 7−8 mg of purified protein per liter of cells. Protein concentrations were measured via optical density at 280 nm using the extinction coefficient of $E_{0.1\%} = 1.8$ calculated from the sequence. The purified protein was stored in 10 mM phosphate buffer (pH 8.0) at 4 °C and used within 2 weeks of the initial purification. The purity of the protein preparations was assayed by SDS−PAGE and by electrospray mass spectrometry (Micromass Quattro II).

Intrinsic Tryptophan Fluorescence Measurements. Fluorescence measurements were made with a FluoroMax-2 fluorescence spectrometer (Jobin Yvon-Spex). Emission spectra between 300 and 420 nm were collected with excitation at 280 nm. Spectra were collected at different pHs within the range of 10−2 using 0.5 μM protein samples in 50 mM of the appropriate buffer containing 100 mM NaCl. Spectra were collected at 25 and 37 °C. The stability of SMA toward urea denaturation was monitored as a function of pH by recording changes in tryptophan fluorescence intensity upon excitation at 280 nm and emission at 350 nm at 25 °C.

Samples of SMA (1 μM monomer) were incubated in 20 mM phosphate buffer (pH 7.4), 100 mM NaCl containing varying amounts of urea (0−8 M) for 2 h to ensure completion of the unfolding reaction. Data were analyzed by nonlinear least-squares fitting to a two-state folding model. The fraction unfolded, F_u, was calculated using the equation: $F_u = (y_f - y)/(y_f - y_u)$ where y represents the observed fluorescence at a particular concentration of urea, and y_f and y_u represent the corresponding fluorescence of the folded and unfolded states, respectively, at that urea concentration. For baseline fitting, a linear least-squares analysis was performed to determine the values of y_f and y_u as a function of urea concentration. The free energies of unfolding were calculated as a function of urea concentration using the equation: $\Delta G = -RT \ln K_{eq}$, where $K_{eq} = f_u/(1 - f_u)$. $\Delta G°$ was determined by linear extrapolation to zero urea concentration using the expression: $\Delta G° = \Delta G + m$[urea].

ANS Binding. 1,8-Anilinonaphthalenesulfonate was obtained from Kodak, and a stock solution was prepared by dissolving in water followed by filtration through a 0.2 μm syringe filter and measuring the concentration using an extinction coefficient of 5000 M^{-1} cm^{-1} at 350 nm. The fluorescence emission spectra of solutions of 10 μM ANS and 0.5 μM protein were collected between 420 and 600 nm upon excitation at 380 nm as a function of pH at 37 °C.

Circular Dichroism Spectra. CD spectra were collected on an AVIV model 62DS spectrometer between 260 and 190 nm for the far-UV region and between 320 and 250 nm for the near-UV region, with a step size of 0.5 nm and an averaging time of 5 s and collecting 5 repeat scans. Cells of 1 and 0.01 cm path length were used for near- and far-UV CD measurements with protein concentrations of 0.5 and 1.7 mg/mL, respectively.

pH Dependence. pH-dependent changes in spectroscopic data were fit using a modified Henderson−Hasselbalch equation for one (eq 1) or two (eq 2) transitions, to determine the midpoints of the transitions:

$$Y_{obs} = \frac{Y_N + Y_{I_U} 10^{pH - pH_{m2}}}{1 + 10^{pH - pH_{m2}}} \quad (1)$$

$$Y_{obs} = \frac{Y_N + Y_{I_N} 10^{pH - pH_{m1}} + \frac{Y_{I_U}}{10^{pH - pH_{m2}}}}{1 + 10^{pH - pH_{m2}} + \frac{1}{10^{pH - pH_{m2}}}} \quad (2)$$

where Y_{obs} is the observed spectroscopic property, Y_N is the

value of the spectroscopic property for the native state, Y_{I_N} is the spectroscopic property for the nativelike intermediate, and Y_{I_U} is the spectroscopic property for the unfolded-like intermediate. pH_{m1} and pH_{m2} are the midpoints of transitions from the native state to the I_N intermediate and from I_N to the I_U intermediate, respectively (*36*).

Thin film ATR-FTIR measurements were performed using a SPECAC out-of-compartment ATR accessory and a Nicolet 800SX FTIR bench. A germanium crystal IRE was used for making hydrated thin films of ~50−100 μg of protein from both soluble and insoluble protein as previously described (*14, 15*). ATR-FTIR spectra were collected followed by Fourier transformation of the sample spectra using a clean crystal spectrum as a background. The water vapor spectrum was collected by reducing the air purge and subtracted from the protein spectrum until the spectra were featureless in the region between 1700 and 1800 cm^{-1}. ATR-FTIR spectra for SMA were collected at pH 7.5 in 50 mM sodium phosphate, 100 mM NaCl, at pH 5.0 in 50 mM sodium acetate, 100 mM NaCl, and at pH 2.0 in 20 mM HCl, 100 mM NaCl. Buffer spectra were subtracted from the sample spectra. Component spectra were obtained by first determining peak positions using both second-derivative and Fourier-self-deconvoluted spectra, followed by curve-fitting to the raw spectrum (*16*).

In Vitro Fibril Formation Assays. Fibril formation was monitored using a fluorescence assay based on the enhanced fluorescence of the dye Thioflavin T (TFT) on binding to amyloid fibrils (*17*). Amyloid fibrils were grown from purified protein (40 μM) in 50 mM buffer and 100 mM NaCl. A filtered protein sample (using 0.22 μm syringe filters) was incubated under the desired conditions in a 1.8 mL flat-bottomed screw-capped glass vial with moderate stirring using a Teflon-coated micro-stir bar. Typical fibril growth experiments involved incubating the protein at 37 °C with constant stirring and removing aliquots (10 μL) over time for analysis by light scattering and TEM and TFT binding (see below). Standard buffers included 20 mM HCl or phosphate (pH 2), 50 mM formate (pH 3 and 4), 50 mM cacodylate or acetate (pH 5 and 6), and 20 mM TRIS or 20 mM HEPES or 50 mM phosphate (pH 7). Both Rayleigh light scattering and fluorescence spectra were collected using a SPEX/Jobin-Yvon Fluoromax-2 spectrofluorometer. Constant temperatures were maintained using a circulating water bath. At each time point, a 220 μL sample was removed and transferred to a cylindrical quartz microcell to measure Rayleigh light scattering at 330 nm with a 1 nm band-pass for both excitation and emission monochromators. Thioflavin T binding assays were conducted by adding sample aliquots (10 μL) to 990 μL of 20 μM TFT in 50 mM TRIS, pH 7.5, and 100 mM NaCl in a 1 mL fluorescence cuvette. Fluorescence emission was monitored with excitation at 450 nm using a 5 nm band-pass on both the excitation and emission monochromators. Fluorescence intensities were reported at 482 nm.

SAXS Measurements. Small-angle X-ray scattering measurements were performed on beam line 4-2 at the Stanford Synchrotron Radiation Laboratory (SSRL) as described previously (*18*). The SAXS instrument was configured with a Mo:CB_4 multilayer monochromator, an 18 mm beamstop, and a 218 cm sample-to-detector distance. Data were collected on protein samples ranging from 0.5 to 10 mg/mL in 50 mM buffer and 100 mM NaCl at 37 °C using a PTFE flow-cell with 1.3 mm path length to minimize radiation damage. Radii of gyration were calculated using the Guinier approximation (*19*).

Atomic Force and Transmission Electron Microscopy. Transmission electron micrographs were collected using a JEOL JEM-100B microscope operating with an accelerator voltage of 80 kV. Typical nominal magnifications ranged from 27000× to 67000×. Samples were deposited on Formvar-coated 300 mesh copper grids and negatively stained with freshly prepared 2% aqueous uranyl acetate.

For AFM, aliquots of 50 μL of incubation solution were transferred to an Eppendorf tube and spun to pellet the precipitated material, which was then washed twice with water before resuspending in deionized water. A drop of aggregate suspension was deposited on freshly cleaved mica and dried immediately with nitrogen gas. The samples were imaged with an Autoprobe CP AFM (Park Scientific, Sunnyvale, CA) in the noncontact (NC-AFM) mode. The tube scanner was a 100 μm Scanmaster (Park Scientific). NC Ultralevers (Park Scientific) were used as cantilevers. The resonant frequency was ~100 kHz. The images were taken in air, ambient conditions, at a scan frequency of 1−2 Hz, using silicon nitride tips.

NMR Spectroscopy. ^{1}H NMR spectra were collected using a Varian Unity+ 500 spectrometer equipped with ultrashims and a Varian triple resonance probe. Presaturation and postacquisition digital filtering were used for solvent suppression. Data were collected on 0.5 mM protein samples containing 100 mM NaCl and 10% D_2O. The pH was adjusted by titration with NaOH or HCl as needed. All data were recorded at 37 °C.

Light Scattering Measurements at High SMA Concentration. The rate of aggregation was monitored by static light scattering using a Nepheloskan instrument from Labsystems and a 96-well plate reader. Solutions of 3.5 and 7 mg/mL SMA at the appropriate pH were incubated at 37 °C along with their corresponding buffers, and scattering was measured every 15 min for 6 h.

pH Jump Experiments. Interconversions between N, I_N, I_U, and U were monitored by diluting 10 μM SMA at one pH into buffer of another pH, such that the final concentration of protein was 1 μM. After manually mixing, the intensity of either tryptophan fluorescence (excitation 280 nm and emission 345 nm) or ANS fluorescence (excitation 380 nm and emission 470 nm) was monitored, using a time-based scan on a Spex Fluoromax instrument with 1 s time-averaging.

RESULTS

Formation of Amyloid Fibrils Is Favored by Destabilizing Environmental Conditions. The enhanced fluorescence emission of the dye Thioflavin T on association with amyloid fibrils provides a very convenient method to monitor the kinetics of amyloid fibril formation (*17, 20*). Fibril formation by SMA was investigated by stirring solutions of SMA at various values of pH at 37 °C. At room temperature, or in the absence of stirring, no enhancement of TFT was observed for several days.

The rate of fibril formation from SMA was found to be very sensitive to a number of extrinsic factors, including pH,

agitation, and temperature. As is typical for other amyloid fibril growth curves, SMA fibrillation kinetics exhibit a quasi-sigmoidal behavior, consisting of a lag phase followed by a logarithmic growth phase that eventually plateaus (Figure 1). The slight drop in TFT fluorescence sometimes observed at long time periods may reflect conversion of the mature SMA amyloid fibrils to an alternative fibrillar form that has a lower affinity toward TFT. For example, we frequently observed lateral aggregation of mature fibrils coinciding with the decrease in TFT fluorescence, suggesting a possible decrease in the availability of TFT binding sites.

We confirmed that the enhanced fluorescence emission of TFT was indeed due to interaction with SMA amyloid fibrils by the characteristic Congo red green-birefringence observed under crossed-polarization (data not shown) and by direct observation with transmission electron microscopy and atomic force microscopy. These techniques demonstrated the presence of fibrils in systems with high TFT fluorescence, and their absence in samples with no increase in TFT fluorescence. The TFT assay was shown to be linear over the concentration range of 0 to >12 μg of amyloidogenic protein in the assay solution.

The initial lag in fibril formation (see Figure 1) is often attributed to the slow assembly of a critical nucleus in a nucleation−polymerization mechanism (*21*). The length of the lag (measured by extrapolating the exponential growth phase to zero intensity) during SMA fibril formation was a sensitive function of the pH at which the fibrils were generated. Some typical data are shown in Figure 1. The length of the lag decreased from days at pH 7.0, 37 °C ,for 40 μM SMA, to a few hours at pH 2 (these values for the lag time are very sensitive to the rate of stirring or agitation). In addition, the maximum signal obtained using the TFT assay increased with decreasing pH, indicating that more fibrils were formed at lower pH values (note that the TFT binding assay is performed at pH 7).

Static light scattering was also used to monitor the kinetics of aggregation (Figure 1). Surprisingly, we noted that amorphous aggregation occurred in the same incubation samples of SMA as fibril formation, but at a faster rate. Substantial amorphous aggregation was observed from pH 7 to 4. The amount of amorphous aggregation was proportional to the protein concentration. The amorphous aggregation was observed immediately after starting the stirring at 37 °C as indicated by increased light scattering (Figure 1B,C), whereas the presence of fibrils, as reflected by the increase in TFT fluorescence, was not observed for several days. Confirmation of the fact that this early aggregation was indeed amorphous comes from TEM and AFM micrographs that showed amorphous material and the absence of fibrils (Figure 2). Under certain conditions, e.g., pH 5.0, 37 °C, 100 mM NaCl, 50−60% of the SMA had precipitated (as amorphous aggregate) after 24 h of incubation (based on the absorbance of the supernatant), and no fibrils were visible by microscopy. In contrast, at pH ≤3 essentially all of the precipitate was fibrillar within 24 h. The rate of the increase in the light scattering observed at pH 2 correlated with that of the increase in Thioflavin T fluorescence (Figure 1A), suggesting that the predominant species present in solution was fibrillar. This was confirmed by TEM, which indicated that the aggregates were largely fibrillar, though some amorphous material was present. Interestingly the maximum increase in Thioflavin T fluorescence was significantly less at pH 7 compared to pH 5 and pH 2, which also correlated with fewer fibrils observed by microscopy at pH 7 compared to the lower pH conditions.

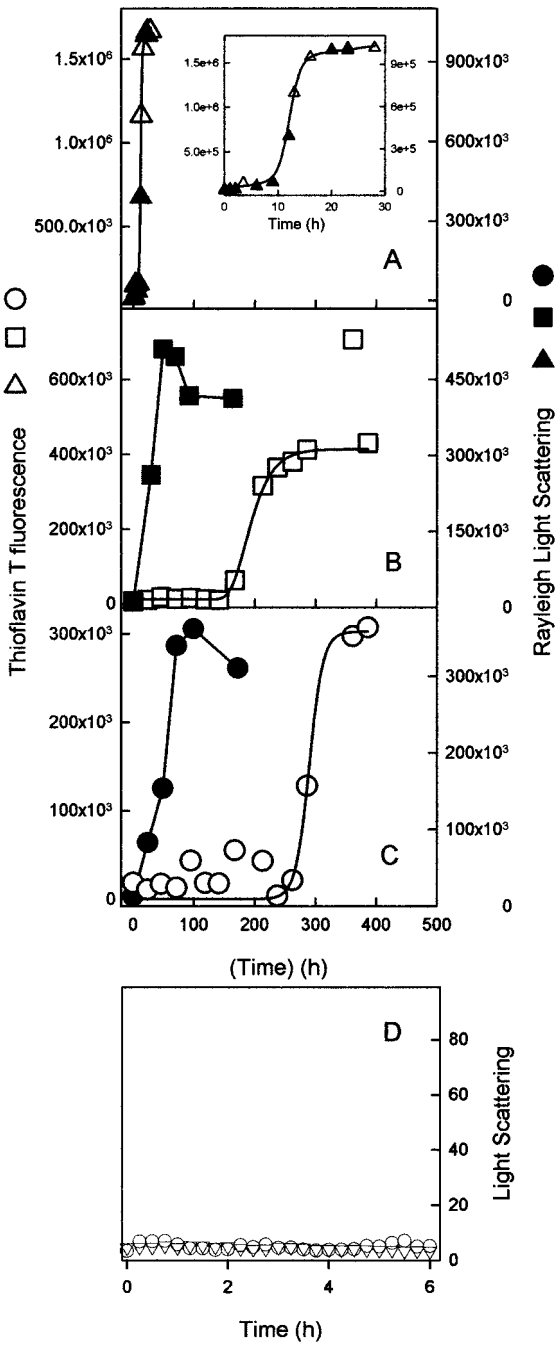

FIGURE 1: pH dependence of amyloid fibril formation by recombinant V_L domain SMA. Fibril formation was monitored using Thioflavin T emission at 482 nm upon excitation at 450 nm at pH 2 (A, △), 5 (B, □), and 7 (C, ○). Rayleigh light scattering was also monitored at pH 2 (A, ▲), pH 5 (B, ■), and pH 7 (C, ●). The formation of amorphous aggregates precedes the formation of amyloid fibrils at pH 7 and 5, conditions that favor the native or the nativelike intermediate conformation. The inset to panel A shows an expanded time scale. Light scattering is sensitive to the presence of both amorphous and fibrillar material, whereas TFT fluorescence is selective for fibrillar aggregates alone. Panel D shows that in the absence of agitation, at SMA concentrations as high as 0.5 mM, no aggregation occurs over at least a 6 h period: circles are for pH 7, triangles for pH 2. With agitation, the signal would be >1400 due to the aggregation.

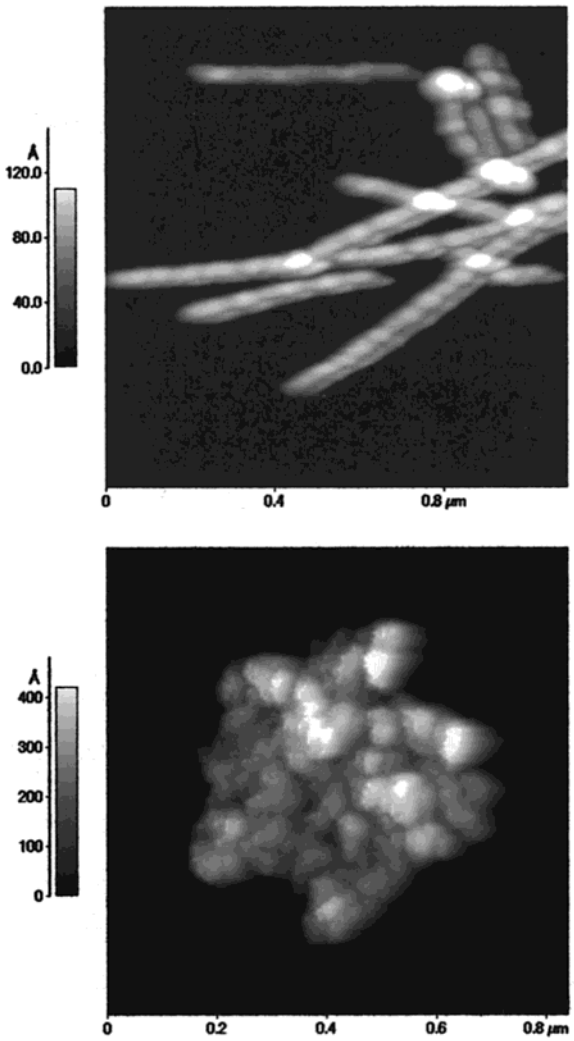

FIGURE 2: Atomic force microscopy images of SMA fibrils observed at pH 2 after 24 h of stirring at 37 °C (A, top). At pH 5 and 7 after incubation for 1 h at 37 °C with constant stirring, a nebulous and loosely packed amorphous deposit is observed (B, bottom). After a few days at pH 5 and 7, both fibrils and amorphous deposits are observed.

Morphology of Fibrillar and Amorphous Deposits. The SMA aggregates were examined using atomic force (Figure 2) and transmission electron microscopy. The images revealed unbranched, rope-like fibrils (Figure 2A), several hundred nanometers in length, most with diameters of ~8 nm, but some, protofibrils, with diameters of ~4 nm (*7*). Upon incubation at 37 °C at pH 4−6, amorphous aggregates were observed (Figure 2B).

Spectroscopic Characterization of Acidic pH Conformations of SMA. A number of spectroscopic probes were utilized to examine conformational changes in SMA that occur under conditions favoring the formation of amorphous aggregates (pH 4−6) and amyloid fibrils (pH <3). Both amyloid fibrils and amorphous aggregates are only formed in solutions of SMA at 37 °C upon agitation of the solution. Note that all the spectroscopic analyses were done at 37 °C without agitation within 2−3 h of preparation, ensuring that only soluble equilibrium conformations were studied; i.e., neither amorphous nor fibrillar aggregates were present in the spectroscopic analyses. No light scattering was observed for at least 6 h for solutions of SMA at concentrations as high as 7 mg/mL (used in the NMR experiments) at various pH

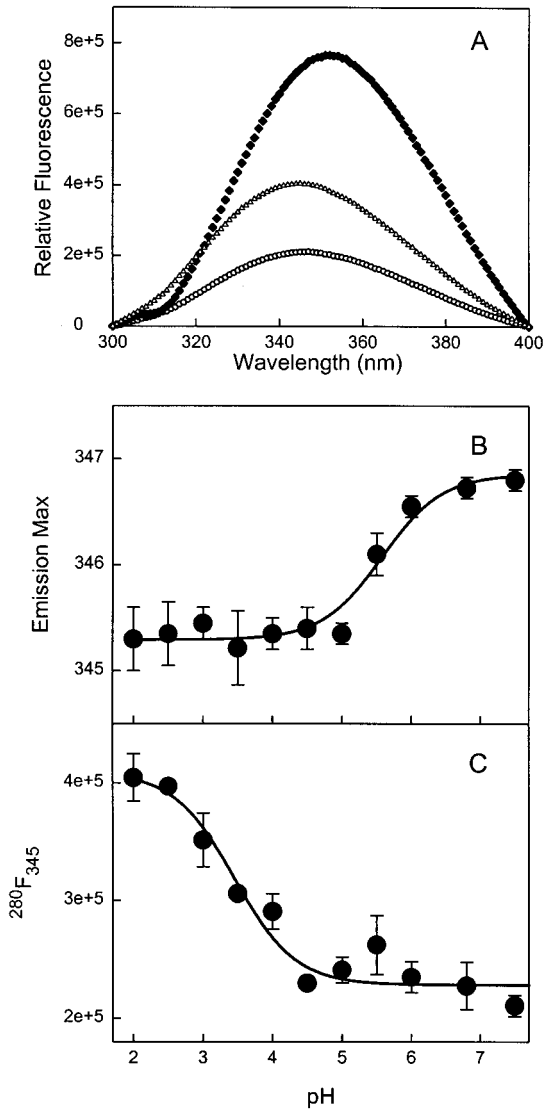

FIGURE 3: Intrinsic tryptophan emission spectra were measured with excitation at 280 nm for 0.5 μM protein solution in 50 mM buffer and 100 mM NaCl at 37 °C for native SMA at pH 7.5 (◆), denatured SMA in 8 M urea at pH 7.5 (○), and I_U at pH 2 (△). The wavelength of maximum emission of tryptophan fluorescence (panel B) and emission intensity (panel C) are plotted against pH. The solid lines are fits to a single ionizable group pH transition using eq 1 (see Materials and Methods). The midpoint of pH transitions for emission maximum and the intensity at 345 nm were 5.6 and 3.5, respectively.

values from 2 to 7 (Figure 1D). Tertiary structure changes were monitored by tryptophan fluorescence emission, near-UV CD, far-UV CD (via the 230 nm peak resulting from aromatic clustering), and by ANS binding studies. Secondary structure changes were monitored by far-UV CD and Fourier transform infrared spectroscopy.

The two tryptophan residues of SMA, W35 and W50, provided convenient spectroscopic means for assessing the protein's conformational state. In particular, W35, which was quenched by the close proximity of the core disulfide formed from C23 and C88 in the native state, was observed to provide a probe of the global conformational state of the V_L domain. Unfolding of the protein resulted in a decrease of the quenching and a consequent increase in the emission intensity of W35 (Figure 3A, and ref *31*). The second tryptophan residue, W50, was solvent-exposed in the native

state, based on both the crystal structure of LEN and the observed λ_{max} of 347 nm in native SMA and LEN.

The intrinsic tryptophan fluorescence spectra indicated λ_{max} of 347 and 355 nm for native and denatured SMA (8 M urea), respectively (Figure 3A). In addition, denatured SMA showed a large increase in Trp fluorescence intensity compared to that of its native conformation. When the pH of a solution of SMA was lowered from 7.5, significant changes were observed in the tryptophan fluorescence emission properties. In the pH 4−6 region, there was a decrease in λ_{max}, from 347 to 345 nm (Figure 3B), which was attributed to the build-up of a partially folded intermediate. For reasons to be discussed below, this intermediate was called I_N (for nativelike intermediate). These data were fit to eq 1, and the midpoint of this pH transition was calculated to be 5.6. At pH <4, the emission intensity increases but the λ_{max} does not change further (Figure 3B,C). The increase in emission intensity observed from pH 5 to 2 suggests significant disassembly of the hydrophobic core of the protein. The midpoint of this transition was pH 3.4 and appeared to be cooperative (Figure 3C). The fluorescence spectrum of SMA at pH 2 had a fluorescence intensity between those of the native and denatured states, and a blue shift in the maximum emission to 345 nm. This suggested that substantial residual structure was present at pH 2. This conformation of SMA, populated below pH 3, was called I_U. In addition, the fluorescence spectrum of SMA was measured as a function of protein concentration, over the 0.05−0.5 mg/mL range, to confirm the presence of the two intermediates and to demonstrate the lack of association of the samples under the experimental conditions.

The near-UV CD spectrum of SMA contained significant contributions from the aromatic (tryptophan, tyrosine, and phenylalanine) residues that were sensitive to the tertiary structure of the protein. The near-UV CD spectrum of native SMA (Figure 4A) showed positive peaks at 286 and 296 nm. These likely reflected contributions from two aromatic clusters involving residues Y36, Y86, Y87, F98 and Y27(d), Y32, Y49, Y91, Y92, observed in the crystal structure of LEN which would also be expected to be present in SMA. The peaks at 286 and 296 nm disappeared with transition midpoints of pH 3.2 and 3.4, respectively (Figure 4B). These transitions correspond to the formation of the I_U species, suggesting loss of the nativelike environment of the aromatic groups in this intermediate. The small positive ellipticity for SMA at 268 nm showed transitions with midpoints of 4.9 and 3.7, corresponding to the transitions to I_N and I_U, respectively (Figure 4B). At pH 2, the near-UV CD spectrum of SMA was essentially featureless (Figure 4A), suggesting loss of most of the tertiary structure in I_U, including the aromatic clusters. As a whole, the near-UV CD spectra for SMA in the pH 4−6 region indicated that the underlying tertiary structure is still relatively nativelike in this pH range, consistent with the presence of a nativelike conformation in I_N.

The hydrophobic dye ANS has frequently been used as a probe to reveal the presence of partially folded intermediates due to the presence of increased exposure of contiguous hydrophobic surface area (*22*−*24*). ANS did not significantly bind to SMA in its native state, indicating the absence of exposed hydrophobic pockets. However, a pH-titration of SMA in the presence of ANS at 37 °C revealed a marked

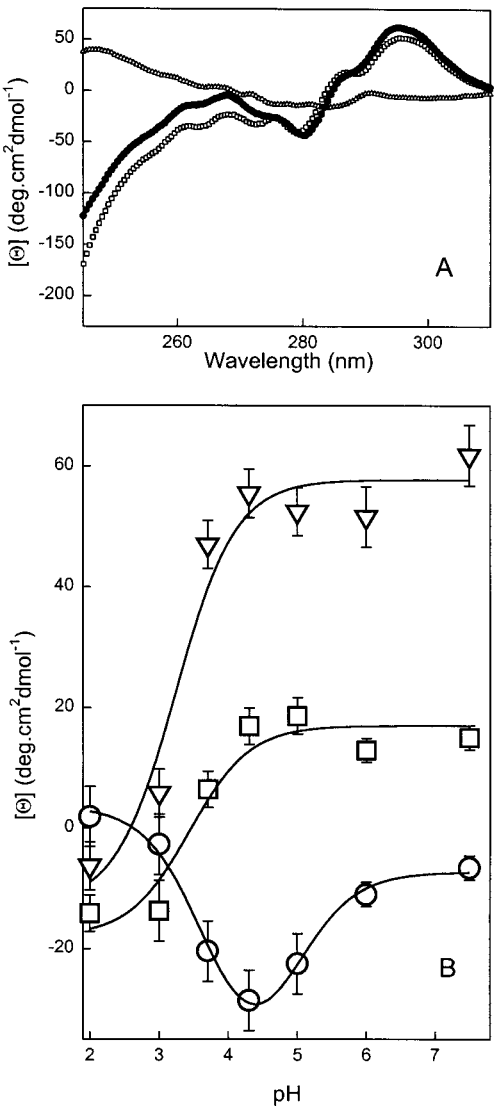

FIGURE 4: Near-UV CD spectra for SMA. Panel A shows plots of molar ellipticity for pH 7.5 (●), pH 5 (□), and pH 2 (△). Panel B shows the pH dependence of the molar ellipticity at 296 nm (▽), 287 nm (○), and 268 nm (□). The lines through the data are fits to eq 1 for peaks at 296 and 287 nm, yielding apparent pK_as of 3.2 and 3.4, respectively, which correspond to formation of I_U. The data at 268 nm are fitted to eq 2, resulting in two apparent pK_a values of pH 4.9 and 3.7. Protein concentration was 0.7 mg/mL.

increase in the fluorescence emission and a blue shift in the ANS emission maximum from 510 to 480 nm. Both the emission intensity increase (data not shown) and the blue shift of the emission were indicative of exposed hydrophobic regions in the vicinity of pH 4−6, with a maximum at pH 4.5 (Figure 5). Such an observation was taken to indicate the build-up of a partially folded intermediate, I_N. The midpoints of the transitions observed for SMA were at pH 5.2 and 3.8 (Figure 5). The limited ANS binding at low pH was attributed to the second intermediate, I_U, which appears to have less contiguous exposed hydrophobic regions. The data suggest that the I_N intermediate is maximally populated between pH 4 and 5 for SMA. In contrast, no ANS binding was observed in the pH 2−10 range for the nonamyloidogenic homologue LEN, indicating the absence of both intermediates with LEN (Figure 5). In addition, the structure of LEN at pH 2 is nativelike, based on small-angle X-ray

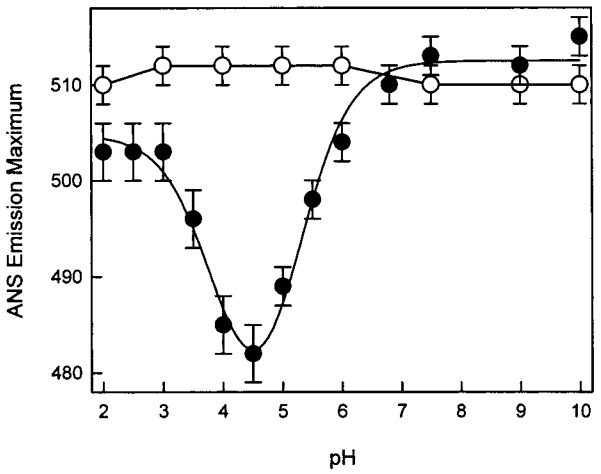

FIGURE 5: pH dependence of binding of ANS to SMA (●) and LEN (○). The reaction was monitored with 0.5 μM protein solution and 10 μM ANS, with excitation at 380 nm. Fluorescence emission spectra were collected between 400 and 600 nm at different pHs. The solid line is a fit to two transitions using eq 2 (see Materials and Methods). The midpoints of the pH transitions were 5.2 and 3.8, respectively.

scattering, circular dichroism, FTIR, and Trp fluorescence (unpublished observations).

Circular dichroism spectra were collected for SMA from pH 8 to 2 to probe global secondary structural changes in the different conformers. The far-UV circular dichroism spectrum of native SMA at pH 7.5 was rather unusual, in that it had distinct minima at 230 nm, as well as at 216 nm (Figure 6A). The former was attributed to contributions from aromatic interactions and possibly the disulfide, the latter to β-structure. When the CD spectrum of SMA was examined as a function of pH at 37 °C, there were relatively small changes between pH 7.5 and pH 4, with more significant changes occurring at lower pH (Figure 6). The former are consistent with loss of some tertiary structure in I_N. The spectrum at pH 2 was significantly different from the spectrum of SMA denatured in 7 M urea or 5 M Gdn·HCl at pH 7.4, indicating significant structure at pH 2. Plots of the ellipticity at 230 nm against pH reveal the population of a distinct conformational species in the pH 4−6 region (Figure 6B). The ellipticity of SMA monitored at 216 nm (corresponding to β-sheet structure) indicated no change between pH 7.5 and 4.0, suggesting that I_N is relatively nativelike. However, below pH 4.0, the negative ellipticity at 216 nm shifted toward lower wavelengths, consistent with the loss of β-sheet structure (Figure 6C). The spectrum at pH 2.0 was a mixture of contributions from β-sheet and random coil conformations, indicating some loss of nativelike β-structure at pH 2. The data were consistent with the presence of a relatively unfolded-like intermediate, I_U, at pH below 3.

Fourier transform infrared spectroscopy (FTIR) has been used to probe protein structure, and the amide I band (1600−1700 cm^{-1}) has been used to estimate protein secondary structure content (*25*). The ATR-FTIR spectra of hydrated thin films of SMA at pH 7.5 and 5 revealed that significant secondary structural changes occur for the I_N intermediate compared to the native state (Figure 7). The major differences are an increase in low-frequency β-sheet (1625 cm^{-1}), an increase in disordered structure (1648 cm^{-1}), increased turn

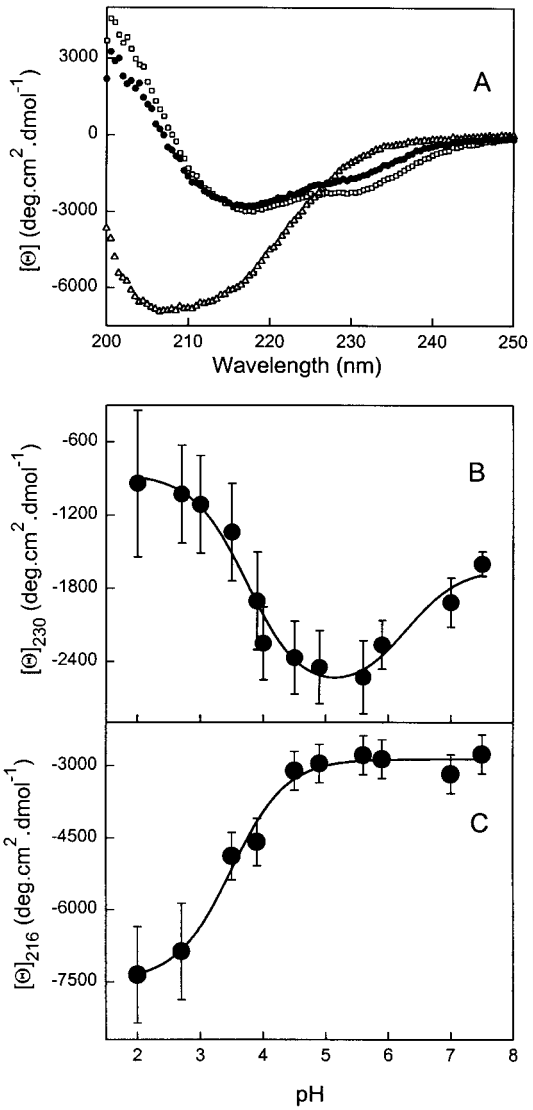

FIGURE 6: Far-UV CD spectra of SMA as a function of pH. Panel A shows the spectra at pH 7.5 (●), pH 5 (□), and pH 2 (△). The changes in molar ellipticity at 230 nm and at 216 nm are plotted against pH in panels B and C, respectively. The solid line in panel B is a fit to eq 2 and gives apparent pK_as of 6.3 and 3.7. The solid line in panel C is a fit to eq 1 and gives an apparent pK_a of 3.5.

(1672 cm^{-1}), and a small decrease in the 1695 cm^{-1} β-component.

At pH 2.0, the amide I spectrum of I_U is different from that at pH 7.5 or 5.0, indicating that I_U has a different secondary structure from native and I_N. The major changes are a large increase in the looplike structure at 1660 cm^{-1} and loss of the major β-peak at 1638 cm^{-1} in the native spectrum, which is replaced by a new, lower intensity β-component at 1631 cm^{-1}.

^{1}H NMR spectra were collected to further assess the conformational changes that took place in SMA at intermediate and low pH. As shown in Figure 8A, the NMR spectrum of SMA at pH 7.0 is characteristic of a tightly folded protein, having well-dispersed amide, aromatic, and aliphatic proton resonances. As the pH was reduced to below pH 5 (Figure 8B), only minor changes in the spectra were observed. These changes included both sharpening of many resonance lines as well as changes in some amide proton chemical shifts. However, the spectrum was still characteristic of a well-

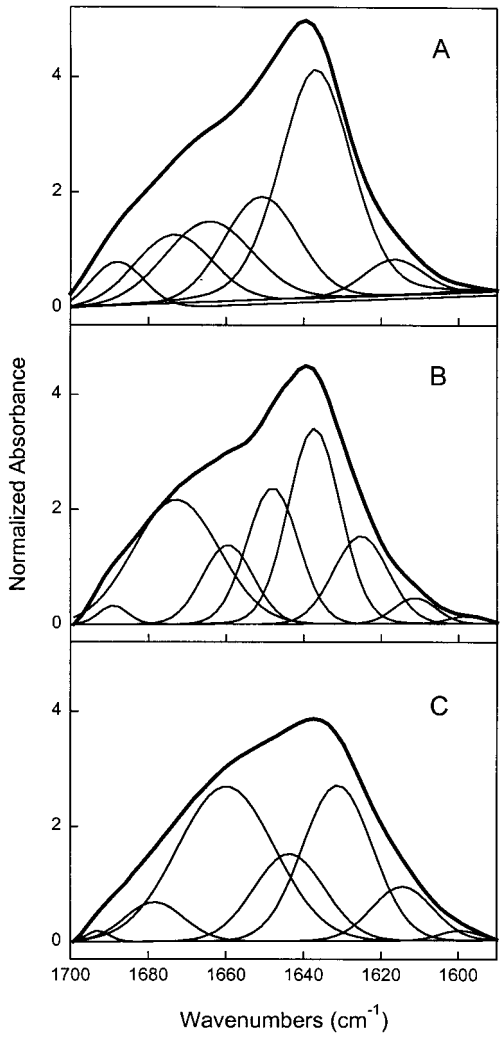

FIGURE 7: Amide I region of the FTIR spectrum of SMA. Panel A shows the spectrum for native SMA at pH 7.5. Panel B shows the spectrum of the nativelike intermediate (I_N) at pH 5.0, and panel C shows the spectrum of the unfolded-like intermediate (I_U) at pH 2.0. The raw ATR-FTIR spectra after water vapor subtraction are shown as thick lines. The thin lines in each panel are the component spectra obtained after curve-fitting the raw spectra.

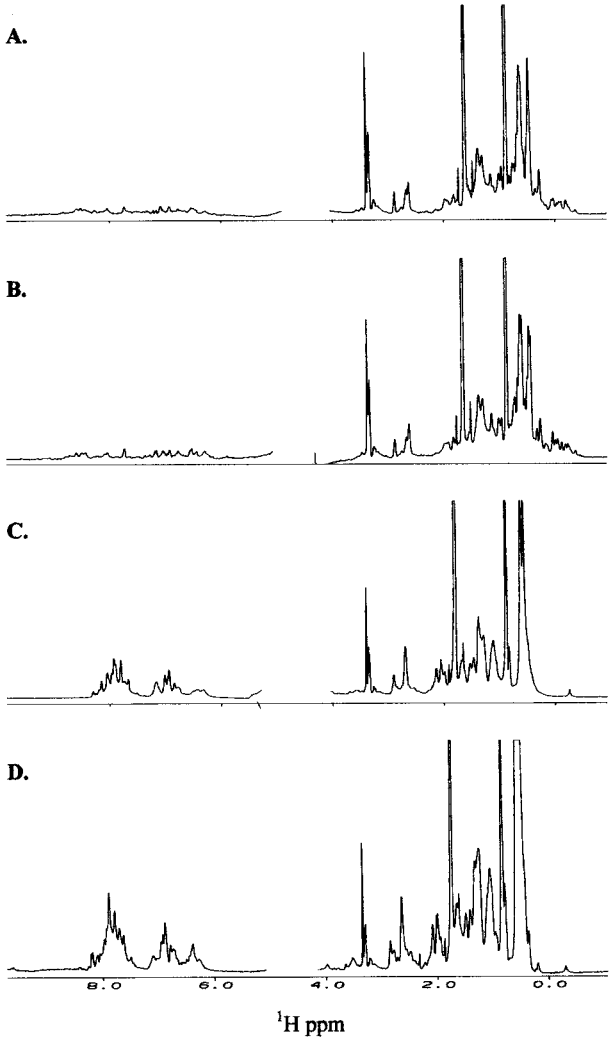

FIGURE 8: ^{1}H NMR spectra of SMA. Panel A shows the spectrum of the native protein at pH 7. Panel B shows the spectrum of the nativelike intermediate, I_N, at pH 5, and panel C the spectrum of the relatively unfolded intermediate, I_U, at pH 2. For comparison, the spectrum of the unfolded protein in 8 M urea, pH 2, is shown in panel D.

folded protein. When the pH was adjusted to below 3, however, the chemical shift dispersion was lost, with the amide proton resonances collapsing to an envelope less than 1.5 ppm wide (Figure 8C). The upfield methyl resonances were also lost below pH 3, with both the aromatic and aliphatic proton regions of the spectrum showing considerable loss of dispersion. Notably, no resonances corresponding to either of the tryptophan indole moieties were apparent in the low-pH spectra. Additionally, the spectrum at pH 2.0 was considerably different from that recorded for SMA under strongly denaturing conditions (pH 2, 8 M urea) as shown in Figure 8D. Under these strongly denaturing conditions, a further loss of dispersion occurs throughout the spectrum, and significant changes in the chemical shifts of nearly all of the amide protons occur. As the solution pH is lowered, the NMR spectra show an increase in signal-to-noise for the same concentration of protein. This is likely due to dissociation of the V_L dimer ($K_d = 40$ μM at pH 7) at lower pH.

Small-Angle X-ray Scattering Characterization of SMA Conformations. Small-angle X-ray scattering measurements indicated that SMA became less compact as the pH was reduced from 7 to 2 (at a protein concentration of 80 μM), with an increase in R_g from 19.6 $\pm$ 0.4 Å at pH 7 to 26.8 $\pm$ 0.6 Å at pH 2. At pH 5, the protein was only slightly expanded, having a R_g of 20.5 $\pm$ 0.6 Å. Kratky plots of the scattering data indicated that extensive globularity was maintained even at low pH, although some denaturation was apparent at pH 5 and more so at pH 2. The significant compactness of I_U ($R_g = 26.8$ Å) is apparent by comparison of its R_g to that of the fully unfolded protein ($R_g > 30$ Å).

Equilibrium Thermodynamic Stability of SMA. The stability of SMA was measured at different pHs using urea denaturation monitored by intrinsic tryptophan fluorescence and far-UV CD. Tryptophan fluorescence had the advantage that it permitted the use of low protein concentrations, which eliminated potential aggregation problems during unfolding. At pH 7.5, SMA is only marginally stable, with a free energy of unfolding $\Delta G° = 4.8$ kcal/mol and $m = 1.05$ kcal/mol. Similar equilibrium plots were obtained when starting with either native or unfolded protein, indicating that there was no hysteresis in the urea unfolding transitions. As the pH was decreased, the stability of SMA decreased significantly (Table 1) as indicated by the decrease in the midpoint of

Table 1: Effect of pH on the Stability of SMA[a]

pH	C_m (M)
2	~0
4	1.5 ± 1.5
6	3.2 ± 0.1
8	4.0 ± 0.1
10	3.5 ± 0.1

[a] Midpoints of urea unfolding transitions were monitored by Trp fluorescence.

the urea unfolding transition with decrease in pH. In light of the evidence for formation of a non-native species from SMA in the vicinity of pH 4−6 (I_N), the urea unfolding data were not converted into free energy data except for neutral pH.

Kinetics of Interconversion of Intermediates. The rates of interconversion between the native conformation (N) and the partially folded intermediates (I_N and I_U) were monitored by pH jumps. Interconversions between N and I_N were monitored using changes in the ANS fluorescence and jumping the pH of solutions of SMA from 7 to 5 (N to I_N) and from 5 to 7 (I_N to N). Interconversions involving I_U were followed by observing changes in the tryptophan fluorescence, with pH jumps of 7 to 2 (N to I_U), 5 to 2 (I_N to I_U), 2 to 5 (I_U to I_N), and 2 to 7 (I_U to N). The results from these experiments show that conversion of N to I_N and I_N to N are fast processes, complete within the dead time of manual mixing, indicating that the rate constant is >0.35 s^{-1}. On the other hand, conversion of either N or I_N to I_U and the reverse are slower processes. The rates for both N to I_U and I_N to I_U were the same within experimental error, namely, 0.01 ± 0.002 s^{-1}, consistent with I_N lying on the pathway between N and I_U. The rates of the transformation of I_U to either I_N or N were the same, with a rate constant of 0.002 ± 0.0008 s^{-1}, again consistent with I_N lying on the pathway between N and I_U.

DISCUSSION

There is increasing evidence to suggest that protein aggregation, including amyloid fibril formation, arises from a partially folded conformation of the aggregating protein (*5, 6, 26*−*30*). The present data strongly support such a hypothesis for the aggregation of immunoglobulin light chain variable domains. Protein aggregation has generally been regarded as being driven by nonspecific hydrophobic interactions operating on unfolded or collapsed molten-globule states. On the other hand, extracellular aggregation of some proteins to form amyloid fibrils has been conventionally attributed to mutations altering the local surface properties of the native state, thereby introducing new packing interactions for oligomerization of the native state (*26*, *31*). In the case of SMA, our results clearly indicate that a nativelike conformation in the fibrils is highly unlikely. Thus, the model for light chain amyloid fibrils proposed by Stevens and coworkers (*31*), and based on the native structure, is inconsistent with the experimental observations.

The partially folded conformations that are the critical precursors to protein aggregation may arise either during the folding of newly synthesized proteins, as with inclusion bodies, or from the native state, as appears plausible for the extracellular amyloid deposits. The build-up of the soluble precursor that triggers aggregation could involve a combination of factors including an amino acid sequence leading to a relatively less stable native state as compared to that of a nonaggregating variant and/or the presence of mildly destabilizing extrinsic conditions.

Detailed analysis of the properties of the amyloidogenic SMA, including its stability, conditions necessary to populate partially folded intermediate conformations, propensity to aggregate, and kinetics of aggregation and fibril formation, provides insight into the molecular basis for aggregation. The present results raise a number of interesting questions, such as: Which features are responsible for the propensity to form fibrils? Why are both amorphous and fibrillar aggregates formed, and what is the relationship, if any, between them? How do the two partially folded intermediate conformations, I_N and I_U, fit into the picture? We will begin with this last question.

Destabilizing Conditions Lead to Partially Folded Intermediate Conformations. Mildly destabilizing conditions, such as low pH or low urea concentrations (data not shown), lead to enhanced aggregation and fibrillation of SMA. The results of the spectroscopic investigations of SMA as a function of pH reveal that SMA forms two partially folded conformations, I_N and I_U, the former being relatively nativelike in its structural properties, whereas the latter is considerably more unfolded. The major significance of the observation of these species is the correlation between formation of amorphous aggregates and I_N, and formation of fibrils and I_U. Both I_N and I_U are envisaged as ensembles of conformations that retain some nativelike structure (more in I_N and less in I_U) with the remainder of the chain, especially for I_U, being highly mobile, and disordered but biased toward its native conformation.

The near- and far-UV circular dichroism, Trp fluorescence, NMR, and SAXS data all point to I_N as being a relatively nativelike species with most structural properties similar to those of the native state. The significant increase in ANS binding, however, points to the critical feature of this intermediate, namely, increased exposure of hydrophobic surfaces compared to the native state. The increased negative ellipticity in the far-UV CD at 230 nm is related to this as it probably represents minor structural rearrangements in side-chain packing manifested as changes in the CD contribution of aromatic residues, rather than secondary structure changes. The enhanced ANS binding in the pH 4−6 range is very consistent with the population of a partially folded intermediate (*22, 23*). Likewise, the FTIR spectrum for I_N reveals that although the overall secondary structure is quite similar to that of the native state, nevertheless there are significant structural differences. These include increased turn structure and a shift in some of the β-structure to components with a lower frequency band, perhaps signifying changes in the β-strand interactions. From examination of the spectral probes as a function of pH, it is apparent that there is a structural transition with a midpoint around pH 5.5. This transition, which corresponds to the interconversion of the native state to I_N, could reflect the titration of histidine or carboxylate residues in SMA. The pH-dependent transition from N to I_N was not observed for the nonamyloidogenic LEN (Figure 5 and unpublished observations). The only differences in ionizable side chains between LEN and SMA are two histidines present in SMA (*8*); this suggests that one

or both of these His residues, either directly or indirectly, may be responsible for the transitions between N and I_N.

The data indicate that SMA forms a second, more unfolded, intermediate, I_U, at pH <3. From comparison of the spectral probe signals as a function of pH, a common transition, attributed to that of I_N to I_U, with a midpoint in the vicinity of pH 3.3 is observed with all the probes. This intermediate retains substantial compactness, and secondary structure, consistent with the presence of a partially folded intermediate conformation. Based on the apparent p*K* of the transition between I_N and I_U, this conformational change is apparently governed by the titration of carboxylate groups. The fact that at pH 2 the fluorescence signal reflects substantial residual structure (significantly decreased intensity and blue-shifted λ_{max} relative to the unfolded and native states) suggests that there is also tertiary structure present in I_U. However, the near-UV CD spectrum indicates the loss of most of the native aromatic side-chain interactions, suggesting that the aromatic clusters present in the native conformation may no longer be present. The FTIR spectra indicate additional loop/disordered structure in I_U compared to the native and I_N conformations and also loss of nativelike β-structure. The NMR spectrum of this intermediate also clearly indicates that it retains considerable secondary and tertiary structure.

Among the factors that stimulate fibril formation from SMA are increased protein concentration, agitation, and increased temperature. All these are likely to result in increased concentration of non-native conformations (through equilibrium between native and non-native states, denaturation at air−water interfaces, and shifting of the equilibrium from native to non-native conformations, respectively), with their known propensity to aggregate. These observations strengthen the correlation between aggregation and precursor partially folded intermediates.

A minor complication in some of these experiments arises from the fact that V_L domains are known to dimerize in a fashion similar to the association of the C_L/V_L domain interaction in intact immunoglobulins. Stevens and Schiffer (*32*) demonstrated that native SMA exists in a monomer−dimer equilibrium with $K_d = 40\ \mu$M under physiological conditions. Thus, data collected with high concentrations of SMA, such as SAXS and NMR, will be potentially complicated by the presence of these native dimers, at least at neutral pH. The main anticipated effect would be that under such conditions the equilibrium between the native conformation and the intermediates would be shifted in favor of the native conformation, rather than a non-native one. This leads to a potential decrease in the rate of fibril formation under conditions where the protein is present mostly as the native dimer (unpublished observations).

Relation between Stability and Aggregation. The stability of SMA is greatly decreased at acidic pH, correlating with both increased amorphous and fibrillar aggregation. The fact that at lower pH SMA readily forms fibrils suggests that removal of nativelike interactions is important prior to fibrillation. Our data show that the aggregation of the amyloidogenic SMA correlates well with the decreased stability of the native state and the population of non-native conformations. We believe that it is the *differential destabilization* of the native state of SMA relative to the partially folded intermediate conformations which is the key feature of the amyloidogenesis, and which will be attenuated in nonamyloidogenic light chains. These observations are in accord with previous investigations of the correlation between amyloidogenesis and stability in light chains, which has indicated that either destabilizing mutations or sequences (*12*, *33*, *34*), or destabilizing conditions (*35*) correlate with increased fibillogenicity. In fact, SMA has been shown to be about 2.5 kcal/molecule less stable than its benign LEN homologue (*8*). Further, it has been shown that destabilizing LEN with Gdn·HCl leads to fibrillation (*12*).

Scheme 1

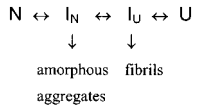

Scheme 2

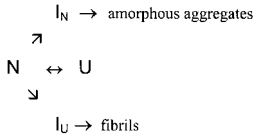

Amorphous and Fibrillar Aggregates. The observation that both fibril and amorphous aggregate formation occur simultaneously under many conditions raises a number of questions, for example: Do they arise from similar or different partially folded conformations, and do amorphous aggregates convert directly or indirectly to fibrils?

The coincident kinetics for light scattering and TFT at pH ≤3, in conjunction with the limited amount of amorphous aggregates observed by EM, indicate that at these low pHs fibrils are preferentially formed, and that the limited amount of amorphous aggregates formed under these conditions rapidly converts to fibrillar species. Since the spectroscopic results suggest that at pH ≤3 the only significant species present is I_U, the limited amount of amorphous aggregates indicates that it is I_U that is responsible for fibril formation. Similarly, the fact that the pH at which maximal amounts of amorphous material is found is in the vicinity of 5.5 indicates that I_N is primarily responsible for the amorphous aggregates. The decreased amplitude of the final TFT signal at higher values of pH is attributed to the increased amount of amorphous aggregate at higher pHs.

The kinetics of interconversion between N, I_N, and I_U are consistent with I_N being on the pathway between N and I_U (Scheme 1). However, the possibility that there are separate pathways to I_N and I_U (Scheme 2) cannot be eliminated at this time. The fast interchange between N and I_N is not surprising, given the fact that I_N is relatively nativelike.

The decreased amounts of fibrils observed at higher pH values presumably result from the smaller amounts of I_U in equilibrium with N and I_N (even though the equilibrium levels of I_U may be quite low at higher pHs, any I_U lost in fibril formation will be replaced by mass action with more soluble I_U). The strong correlation between the pH dependence of aggregation (and fibril formation) and the population of the partially folded intermediates supports the hypothesis that the observed intermediates are key players in the aggregation process. Fibril generation, even under nativelike conditions, can be attributed to the Boltzmann distribution of ensembles of various states under nativelike conditions. Hence, it possible that the key intermediate, highly populated

at pH ≤3, is also present under nativelike conditions, but at substantially lower concentration, and is responsible for amyloid formation after an extended lag period.

Aggregation results from the strong self-association tendency of the partially folded intermediates, probably due to the presence of large solvent-exposed hydrophobic patches, which are absent in the native and fully unfolded states. The increased β-structure observed in the aggregated states reflects β-strand−β-strand interactions involved in the intermolecular association. Fibril formation is expected to involve a number of intermediate states of soluble oligomers of partially folded intermediates, potentially populated at very low levels. Aggregation occurs under conditions in which a suitably high concentration of the key partially folded intermediate is present, due to a combination of destabilizing factors, such as pH and temperature, or urea, and amino acid sequence, as well as the concentration of the intermediate. Thus, it is mostly the intrinsically low stability of SMA that leads to the build-up of the intermediate leading to aggregation, under conditions where more stable light chains form negligible intermediate and remain in the native conformation.

The much more rapid formation of amorphous aggregates of SMA, compared to fibrils, is very interesting, and raises a number of questions regarding the nature of the relationship between the initially formed amorphous aggregates and the more slowly formed fibrils. Based on the data reported here, it is apparent that the partially folded intermediate populated in the pH 4−6 region is the direct precursor of the amorphous aggregates. The correlation between I_N and amorphous aggregates, and I_U and fibrillar aggregates, suggests that the ratio of the two types of deposits is determined, at least in part, by kinetic competition between the pathways leading to the two different intermediates. A more detailed investigation of the relationship between amorphous and fibrillar deposits will be given elsewhere.

The results of the present investigation firmly establish the existence of partially folded intermediates as key precursors on the aggregation pathway of the amyloidogenic light chain variable domain SMA. In addition, the observation of two such intermediates is the first report that a given protein might have more than one critical intermediate conformation on the aggregation pathway, and that such different conformations may lead to different types of deposits. One implication of this is that factors, such as chaperones, which may change the effective concentration of one of the intermediates may change the nature of the deposits.

ACKNOWLEDGMENT

We thank Vladimir N. Uversky and Pierre Soulliac for helpful discussions, Sue Carter for the atomic force microscope, and Sebastian Doniach for assistance with the small-angle X-ray scattering experiments.

REFERENCES

1. Buxbaum, J. (1992) *Hematol. Oncol. Clin. North Am. 6*, 323−346.
2. Buxbaum, J., and Gallo, G. (1999) *Hematol. Oncol. Clin. North Am. 13*, 1235−1248.
3. Kaplan, B., Vidal, R., Kumar, A., Ghiso, J., Frangione, B., and Gallo, G. (1997) *Clin. Exp. Immunol. 110*, 472−478.
4. Buxbaum, J. N., Chuba, J. V., Hellman, G. C., Solomon, A., and Gallo, G. R. (1990) *Ann. Intern. Med. 112*, 455−464.
5. Lai, Z., Colón, W., and Kelly, J. W. (1996) *Biochemistry 35*, 6470−6482.
6. Booth, D. R., Sunde, M., Bellotti, V., Robinson, C. V., Hutchinson, W. L., Fraser, P. E., Hawkins, P. N., Dobson, C. M., Radford, S. E., Blake, C. C. F., and Pepys, M. B. (1997) *Nature 385*, 787−793.
7. Ionescu-Zanetti, C., Khurana, R., Gillespie, J. R., Petrick, J. S., Trabachino, L. C., Minert, L. J., Carter, S. A., and Fink, A. L. (1999) *Proc. Natl. Acad. Sci. U.S.A. 96*, 13175−13179.
8. Stevens, P. W., Raffen, R., Hanson, D. K., Deng, Y. L., Berrios-Hammond, M., Westholm, F. A., Murphy, C., Eulitz, M., Wetzel, R., Solomon, A., Schiffer, M., and Stevens, F. J. (1995) *Protein Sci. 4*, 421−432.
9. Pras, M., Schubert, M., Zucker-Franklin, D., Rimon, A., and Franklin, E. C. (1968) *J. Clin. Invest. 47*, 924−933.
10. Solomon, A. (1985) *Methods Enzymol. 116*, 101−121.
11. Huang, D. B., Chang, C. H., Ainsworth, C., Johnson, G., Solomon, A., Stevens, F. J., and Schiffer, M. (1997) *Mol. Immunol. 34*, 1291−1301.
12. Raffen, R., Dieckman, L. J., Szpunar, M., Wunschl, C., Pokkuluri, P. R., Dave, P., Wilkins, S. P., Cai, X., Schiffer, M., and Stevens, F. J. (1999) *Protein Sci. 8*, 509−517.
13. Skerra, A., Pfitzinger, I., and Pluckthun, A. (1991) *Biotechnology (N.Y.) 9*, 273−278.
14. Oberg, K. A., and Fink, A. L. (1998) *Anal. Biochem. 256*, 92−106.
15. Seshadri, S., Khurana, R., and Fink, A. L. (1999) *Methods Enzymol. 309*, 559−576.
16. Fink, A. L., Seshadri, S., Khurana, R., and Oberg, K. A. (1999) in *Infrared Analysis of Peptides and Proteins* (Singh, B. R., Ed.) American Chemical Society, Washington, DC.
17. Naiki, H., Higuchi, K., Hosokawa, M., and Takeda, T. (1989) *Anal. Biochem. 177*, 244−249.
18. Uversky, V. N., Karnoup, A. S., Khurana, R., Segel, D. J., Doniach, S., and Fink, A. L. (1999) *Protein Sci. 8*, 161−173.
19. Guinier, A., and Fournet, G. (1955) in *Small-angle scattering of X-rays*, p 268, Wiley, New York.
20. Levine, H. (1993) *Protein Sci. 2*, 404−410.
21. Jarrett, J. T., and Lansbury, P. T. (1992) *Biochemistry 31*, 12345−12352.
22. Goto, Y., and Fink, A. L. (1989) *Biochemistry 28*, 945−952.
23. Semisotnov, G. V., Rodionova, N. A., Razgulyaev, O. I., Uversky, V. N., Gripas, A. F., and Gilmanshin, R. I. (1991) *Biopolymers 31*, 119−128.
24. Fink, A. L. (1999) in *The Encyclopedia of Molecular Biology* (Creighton, T. E., Ed.) pp 140−142, John Wiley & Sons, New York.
25. Byler, D. M., and Susi, H. (1986) *Biopolymers 25*, 469−487.
26. Wetzel, R. (1996) *Cell 86*, 699−702.
27. Fink, A. L. (1998) *Folding Des. 3*, 9−15.
28. Speed, M. A., Wang, D. I. C., and King, J. (1996) *Nat. Biotechnol. 14*, 1283−1287.
29. Wetzel, R. (1999) *Amyloid, prions and other protein aggregates*, Academic Press, New York.
30. Quintas, A., Saraiva, M. J., and Brito, R. M. (1999) *J. Biol. Chem. 274*, 32943−32949.
31. Stevens, F. J., Myatt, E. A., Chang, C. H., Westholm, F. A., Eulitz, M., Weiss, D. T., Murphy, C., Solomon, A., and Schiffer, M. (1995) *Biochemistry 34*, 10697−10702.
32. Stevens, F. J., and Schiffer, M. (1995) *Methods Mol. Biol. 51*, 51−81.
33. Wall, J., Schell, M., Murphy, C., Hrncic, R., Stevens, F. J., and Solomon, A. (1999) *Biochemistry 38*, 14101−14108.
34. Bellotti, V., Stoppini, M., Mangione, P. P., Fornasieri, A., Min, L., Merlini, G., and Ferri, G. (1996) *Biochim. Biophys. Acta 1317*, 161−167.
35. Kim, Y., Wall, J. S., Meyer, J., Murphy, C., Randolph, T. W., Manning, M. C., Solomon, A., and Carpenter, J. F. (2000) *J. Biol. Chem. 275*, 1570−1574.
36. Khurana, R., Hate, A. T., Nath, U., and Udgaonkar, J. B. (1995) *Protein Sci. 4*, 1133−1144.

BI001782B